

Planar Topological Hall Effect from Conical Spin Spirals*

Narayan Mohanta,^{1,†} Satoshi Okamoto,¹ and Elbio Dagotto^{1,2}

¹Material Science and Technology Division, Oak Ridge National Laboratory, Oak Ridge, TN 37831, USA

²Department of Physics and Astronomy, The University of Tennessee, Knoxville, TN 37996, USA

Planar Topological Hall effect (PTHE), with an external magnetic field applied in the plane of the charge current, is believed to arise from in-plane skyrmions. Here, we propose that the PTHE can robustly appear also from an unexpected source, the conical spin spiral phase, realizable in a wide variety of materials. We show that for both in-plane skyrmion tubes and conical spin spirals, the PTHE is two-fold symmetric with respect to the magnetic-field angle, while it is four-fold symmetric for labyrinth domains of orthogonal conical spin spirals. We predict that the symmetry and thickness-dependence of the PTHE can distinguish between the two scenarios, unambiguously probing the nature of the antisymmetric spin-exchange interaction and the resulting magnetic texture.

Introduction.—Transport of electrons in the presence of chiral magnetic textures has emerged as a central topic to pave the way towards exciting new physics and spintronics applications [1–3]. In noncentrosymmetric magnets and oxide interfaces, the chiral magnetic textures typically originate from Dzyaloshinskii-Moriya (DM) -type antisymmetric exchange interactions [4, 5]. A non-collinear texture, such as the skyrmion crystal (SKX), possesses a finite scalar spin chirality which produces an emergent magnetic field and influences the electronic transport, giving rise to topological Hall effect in metals [1, 6–17].

In the planar Hall geometry, with coplanar magnetic field and charge current, a field-angular modulation of the planar topological Hall conductivity was proposed to originate from in-plane skyrmion tubes (IST) when the DM interaction has a finite component perpendicular to the plane where the magnetic field is applied, as in non-centrosymmetric magnets [18]. In a wide variety of compounds and heterostructures with broken structural inversion symmetry, the DM interaction is two-dimensional (2D) in nature [15, 19, 20] and lies in the plane of the applied magnetic field. In this scenario, PTHE is unanticipated since the formation of IST is not possible.

Here, we show that conical spin spirals (CSS), the underlying magnetic texture with DM vectors parallel to the plane where the magnetic field is applied, can also generate a significant PTHE. This finding opens up opportunities to elucidate transport properties originating in chiral magnetic textures beyond skyrmions. We find that the PTHE from the CSS is two-fold symmetric with respect to the magnetic-field angle – similar to that from the IST – when only one of the two orthogonal stripe arrangements is present. However, in real magnetic materials, both stripe arrangements often coexist and form labyrinth-like metastable domains, induced by defect pinning. The PTHE in this case of labyrinth stripe domains is four-fold symmetric, clearly distinguishable from the PTHE arising from the IST. Based on the symmetry, magnetic-field dependence, and thickness dependence of the PTHE, we formulate strategies to characterize the nature of the antisymmetric spin-exchange interaction

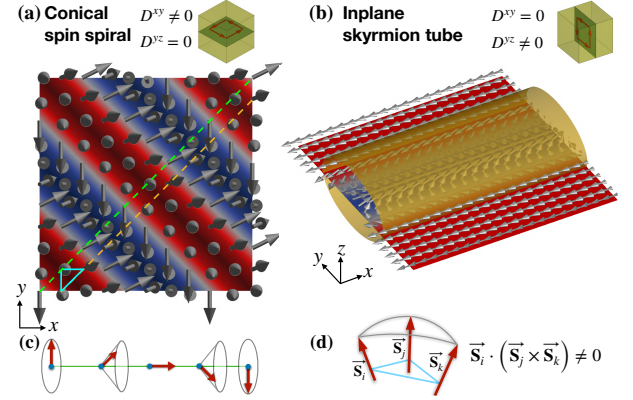


FIG. 1. Schematic spin arrangements in a 2D plane for (a) conical spin spirals originating from in-plane DM vectors and (b) in-plane skyrmion tubes originating from out-of-plane DM vectors. (c) Conical spin arrangement along the green (or yellow) dashed line in (a). (d) In both plots (a) and (b), three spins on some triangular plaquettes, as shown by the cyan triangle in (a), subtend a finite solid angle in real space, creating a finite scalar spin chirality, the source of the PTHE.

which is often difficult to understand only from indirect experimental evidences.

In Fig. 1, we show schematically the two spin textures under consideration, *viz.* the CSS (with DM vectors lying in the x - y plane, *i.e.* $\mathbf{D}^{xy} \neq 0$, $\mathbf{D}^{yz} = 0$) and the IST (with DM vectors lying in the y - z plane, *i.e.* $\mathbf{D}^{xy} = 0$, $\mathbf{D}^{yz} \neq 0$). The key difference is that the DM vectors lie in different planes. In both cases, a finite scalar spin chirality $\chi_{ijk} = \mathbf{S}_i \cdot (\mathbf{S}_j \times \mathbf{S}_k)$, the origin of the PTHE, emerges in some regions of the 2D plane. A finite solid angle subtended by $\hat{n}(\mathbf{r}) = \mathbf{S}(\mathbf{r})/|\mathbf{S}(\mathbf{r})|$, the orientation of the localized spin $\mathbf{S}(\mathbf{r})$, over an infinitesimal loop in space in the continuum limit generates an emergent magnetic field, which can be expressed in two dimensions as $B_z^e = \frac{\hbar}{2e} \hat{n} \cdot \left(\frac{\partial \hat{n}}{\partial x} \times \frac{\partial \hat{n}}{\partial y} \right)$ [1, 13, 22]. In the present context of the CSS or the IST, the scalar spin chirality χ and the emergent magnetic field B_z^e are also finite, and a PTHE is expected to appear asymmetrically with respect to the field angle.

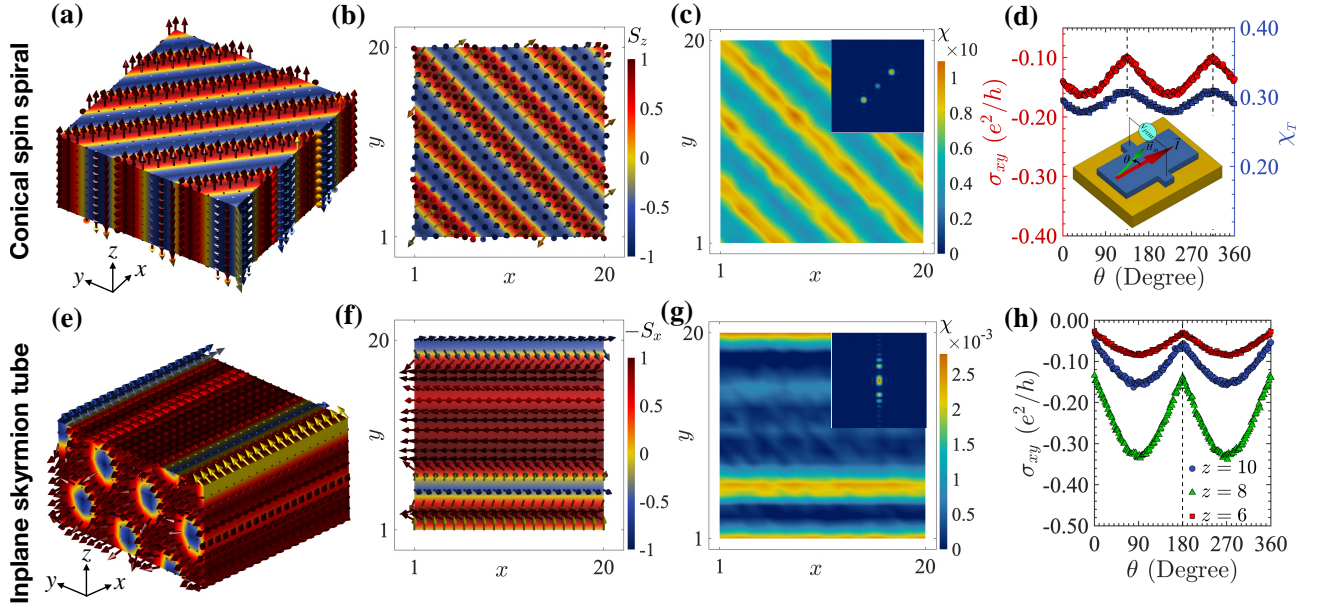


FIG. 2. Monte Carlo-generated spin texture and planar Hall response of the CSS (top row) and IST (bottom row). Spin texture of a $20 \times 20 \times 10$ slab with the DM vectors lying in (a) the x - y plane and (e) the y - z plane. A magnetic field of strength $H_{in} = 0.9J$ is applied along the x direction in both cases. (b) and (f) show the 2D view of the surface ($z = 10$) of the slab, revealing the CSS [in (b)] and IST [in (f)]. (c) and (g) are the profiles of the scalar spin chirality χ for the spin textures in (b) and (f), respectively. Insets in (c) and (g) show the Bragg intensity profile $I(\mathbf{q})$ in the 2D Brillouin zone of the $z = 10$ layer. (d) Monte Carlo-averaged transverse Hall conductivity σ_{xy} (left y axis) and total scalar spin chirality χ_T (right y axis), plotted as a function of the field angle θ , for the CSS. Inset shows the geometry of the PTHE with a charge current assumed to be running along the x direction, the Hall voltage measured along the transverse direction, and the magnetic-field angle θ determined with respect to the current direction. (h) θ -variation of σ_{xy} for the IST case at different thicknesses of the slab. Parameters used are $J = 1$, $S = 1$, $D = \sqrt{6}$, and $T = 0.001$. The value of D was chosen to realize a SkX of small skyrmion size [21].

Model and formalism.—The transverse Hall response in the planar Hall geometry [inset in Fig. 2(d)] is studied here using the chiral magnetic texture of the top surface of a three-dimensional (3D) slab having isotropic ferromagnetic exchange interactions and 2D DM vectors. At zero field and a very low temperature, the spin texture is obtained by using Metropolis Monte Carlo (MC) annealing [21, 23], formulated using the spin Hamiltonian

$$\mathcal{H} = -J \sum_{\langle ij \rangle} \mathbf{S}_i \cdot \mathbf{S}_j - \sum_i \mathbf{H}_{in} \cdot \mathbf{S}_i - \sum_{\langle ij \rangle} \mathbf{D}_{ij}^{\alpha\beta} \cdot (\mathbf{S}_i \times \mathbf{S}_j),$$

where $J > 0$ is the strength of the ferromagnetic Heisenberg exchange, i and j are indices of nearest-neighbor lattice sites in 3D space, \mathbf{H}_{in} is the strength of the applied in-plane magnetic field, and $\mathbf{D}_{ij}^{\alpha\beta} = D(\hat{\alpha} \times \hat{\beta}) \times \hat{r}_{ij}$ represents the DM vector between sites i and j lying in the $\alpha - \beta$ plane, with D being the strength of the DM interaction and \hat{r}_{ij} the unit vector between sites i and j . Below we consider two cases separately: (a) $|\mathbf{D}_{ij}^{xy}| \neq 0$, $|\mathbf{D}_{ij}^{yz}| = 0$ and (b) $|\mathbf{D}_{ij}^{xy}| = 0$, $|\mathbf{D}_{ij}^{yz}| \neq 0$. When adding the in-plane field, the spin textures were obtained by performing the MC evolution starting from the previously MC converged zero-field low-temperature spin configuration, without changing the temperature [23]. Each field angle θ was measured with respect to the x direction.

With the DM vectors lying in the x - y plane, Fig. 2(a) shows the CSS texture, spontaneously generated by the

MC method in a $20 \times 20 \times 10$ slab at $H_{in} = 0.9J$ and $\theta = 0^\circ$. The top surface of the slab, shown in Fig. 2(b), exhibits a nonzero scalar spin chirality profile, presented in Fig. 2(c), calculated via $\chi(\mathbf{r}_i) = \sum_{ijk \in p} |\mathbf{S}_i \cdot (\mathbf{S}_j \times \mathbf{S}_k)|$, where i, j and k are the three sites of a triangular plaquette p in the underlying square lattice that contains site i . The Bragg intensity profile $I(\mathbf{q}) = (1/N) \sum_{ij} \langle \mathbf{S}_i \cdot \mathbf{S}_j \rangle e^{-i\mathbf{q} \cdot (\mathbf{r}_i - \mathbf{r}_j)}$, where N is the total number of lattice sites on the surface of the slab, shows a small peak at $\mathbf{q} = \mathbf{0}$ indicating a small spin polarization [inset in Fig. 2(c)], a characteristic feature that distinguishes a CSS from the regular spin spiral which appears at $H_{in} = 0$.

To calculate the transverse Hall conductivity at the surface of the slab magnetic system, we consider the following double-exchange Hamiltonian

$$\mathcal{H}_{DE} = -t \sum_{\langle ij \rangle} c_{i\sigma}^\dagger c_{j\sigma} - J' \sum_{i, \sigma, \sigma'} (\mathbf{S}_i \cdot \boldsymbol{\sigma}_{\sigma\sigma'}) c_{i\sigma}^\dagger c_{i\sigma'},$$

where t is the nearest-neighbor electron hopping energy and J' is the strength of the exchange coupling between the itinerant electron $\boldsymbol{\sigma}$ and localized \mathbf{S}_i spins. The configuration of localized spins is generated using MC simulations. The transverse Hall conductivity is obtained via the Kubo formula

$$\sigma_{xy} = \frac{e^2}{h} \frac{2\pi}{N} \sum_{\epsilon_m \neq \epsilon_n} \frac{f_m - f_n}{(\epsilon_m - \epsilon_n)^2 + \eta^2} \text{Im} \left(\langle m | \hat{j}_x | n \rangle \langle n | \hat{j}_y | m \rangle \right),$$

where f_m is the Fermi function at temperature T and energy ϵ_m , \hat{j}_x (\hat{j}_y) is the current operator along the x (y) direction, $|m\rangle$ is the m^{th} eigenstate of \mathcal{H}_{DE} , and η is the relaxation rate. We used $t = 1$, $J' = 1$, and $\eta = 0.1$ for the results presented here, with no qualitative difference in the description for other choices, as elaborated before [21]. MC averaging of σ_{xy} was performed by considering 50 different realizations of the spin textures, obtained at a low temperature $T=0.001J$.

PTHE from conical spin spirals.—The Hall conductivity σ_{xy} for the CSS texture, versus the magnetic-field angle θ , is in Fig. 2(d) displaying an anisotropic behavior. The anisotropy arises from the stripes being oriented along one of the diagonals. The field angle where $|\sigma_{xy}|$ is maximized (minimized) corresponds to a field perpendicular (parallel) to the CSS stripes in Fig. 2(b). The total scalar spin chirality χ_T [see the right y axis in Fig. 2(d)] also displays a similar anisotropic behavior, confirming the appearance of a finite PTHE from the CSS texture. Since the DM vectors lie entirely in the x - y plane, the θ -dependence of σ_{xy} is identical for different slab thicknesses of the material. In other words, for 2D DM vectors lying in the plane of the magnetic field the PTHE is independent of the thickness of the magnetic material. This phenomenon is expected to appear at perovskite-oxide interfaces (*e.g.* manganite-iridate interfaces) where the interface DM interaction originates from Rashba spin-orbit coupling [5, 19, 21].

PTHE from in-plane skyrmion tubes.—Now let us address a second scenario, discussed earlier in Ref. [18]. In noncentrosymmetric magnets [24–26] and layered ferromagnets [27, 28], the DM interaction might have a finite component out of plane and an anisotropy, sizable in thin-films, that stabilizes the SkX phase in a plane perpendicular to the magnetic field. The skyrmions form tubes with the tube axis perpendicular to the plane of the DM vectors. Therefore, some of these skyrmion tubes – those that coincide with the top slab surface where the magnetic field is applied – are expected to produce a PTHE, as conjectured before in the context of MnSi [18]. Consider the DM vectors lying in the y - z plane. In the presence of a magnetic field applied along the x axis, a Néel-type SkX phase is stabilized in the y - z plane, as depicted in Fig. 2(e). The IST spin texture on the top surface ($z = 10$) is in Fig. 2(f). The scalar spin chirality χ , plotted in Fig. 2(g), is finite near the skyrmion tubes, oriented along the x direction. The Bragg intensity profile $I(\mathbf{q})$ for the IST texture is in the inset of Fig. 2(g). The transverse Hall conductivity σ_{xy} , plotted in Fig. 2(h) with respect to θ , presents an enhancement when the magnetic field is applied at an angle away from the IST orientation direction *i.e.* along $\theta = 0^\circ$ and $\theta = 180^\circ$.

Even though the topological Hall conductivity arising from the IST texture could be larger than that from the CSS texture, it could be challenging to decipher the nature of the underlying spin texture from its nearly similar

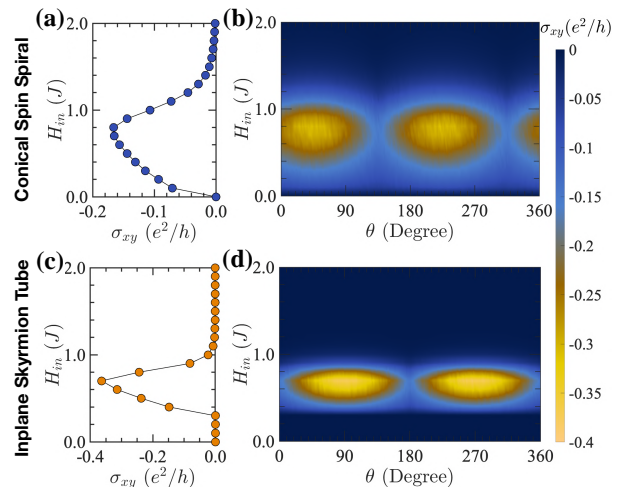


FIG. 3. Variation of the PTHE with magnetic field. MC-averaged transverse Hall conductivity σ_{xy} vs magnetic field amplitude H_{in} for (a) a CSS texture at a field angle $\theta = 0^\circ$ and (c) an IST texture at $\theta = 180^\circ$. Plots (b) and (d) show the variation of σ_{xy} for (b) a CSS texture and (d) an IST texture with field angle θ and field amplitude H_{in} . Other parameters used are as in Fig. 2.

field-angular profile in these two cases, especially when the DM interaction profile has both in-plane and out-of-plane components. Interestingly, based on our calculations on a small slab system, we find that σ_{xy} , at a given field angle θ , varies non-monotonically with the slab thickness, as shown in Fig. 2(h) for three consecutive values of the slab thickness. This result implies a thickness dependence of σ_{xy} , with a period dependent upon the size of the skyrmions. This is in sharp contrast with the planar topological Hall response from the CSS. In a larger system, a similar periodic thickness profile of σ_{xy} is also expected to be observed and this difference could be useful to distinguish the IST from the CSS textures using the PTHE measurements.

Magnetic-field variation of PTHE.—To explore the differences in the PTHE between the CSS and IST cases, we now explore the variation of PTHE with the external magnetic-field amplitude. The SkX phase, with $|\mathbf{D}_{ij}^{yz}| \neq 0$, $|\mathbf{D}_{ij}^{xy}| = 0$, is stabilized in the magnetic slab under consideration within a range of magnetic-field amplitudes, when the field is applied parallel (or anti-parallel) to the in-plane x axis. Consequently, in topological Hall measurements, the formation of the SkX phase is indicated by an enhancement in the topological Hall conductivity within a sharp range of magnetic fields. In Fig. 3, we compare the field-dependence of the planar topological Hall response from the two chiral spin textures investigated in this effort.

For the CSS phase, the transverse Hall conductivity σ_{xy} increases with magnetic field in the low-field regime ($H_{in} \lesssim 0.8J$), and decreases in the high-field regime ($H_{in} \gtrsim 0.8J$), as shown in Fig. 3(a). Such a non-monotonic field-dependence appears from the fact that the CSS

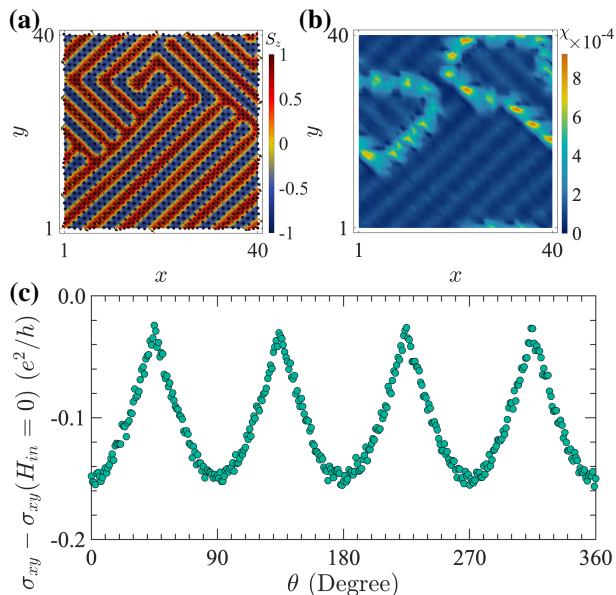


FIG. 4. Labyrinth domains and four-fold symmetric PTHE. (a) MC spin texture of a CSS texture on the surface of the $40 \times 40 \times 6$ slab, showing labyrinth domains of two mutually orthogonal CSS arrangements in an in-plane magnetic field of strength $H_{in} = 0.3J$, applied along the x direction. (b) Spatial profile of the scalar spin chirality χ for the CSS texture shown in panel (a). (c) MC-averaged transverse Hall conductivity σ_{xy} , after subtracting the zero-field value, plotted with respect to the angle θ of the in-plane magnetic field, showing a four-fold symmetry of the PTHE. Other parameters are the same as in Fig. 2.

phase is stabilized within a broad range of magnetic fields, in between the normal spin spiral phase at zero field and the in-plane ferromagnetic phase at very large field, with both of these limits having zero topological Hall conductivity. Figure 3(b) shows a similar enhancement in σ_{xy} at all field angles θ , except near $\theta = 135^\circ$ and $\theta = 315^\circ$ i.e. the alignment direction of the CSS stripes.

On the other hand, σ_{xy} for the IST phase enhances rapidly and remains nonzero only within a sharply-defined field range $0.4J \lesssim H_{in} \lesssim J$. The field range for the IST texture is smaller than that for the CSS texture. Figure 3(d) shows the θ -dependence of the field-variation in σ_{xy} , similar to that in the case of CSS, with the minima located at $\theta = 0^\circ$ and $\theta = 180^\circ$, fixed by the orientation direction of the skyrmion tubes.

Four-fold symmetric PTHE from labyrinth domains.—In general, the spin spirals have two orthogonal solutions which often coexist to form maze-like domain structures, also known as labyrinth domains. These kind of metastable domains can be induced by pinning of the spin spirals by impurities within the sample. The existence of such labyrinth domains was reported in several compounds (both bulk and heterostructures), including thin ferromagnetic films [29–32] and noncentrosymmetric magnets [7, 33], in the absence of any magnetic field [23]. In Fig. 4(a), we show the surface spin texture with do-

main of CSS textures formed in a $40 \times 40 \times 6$ slab – with a larger lateral dimension than the previously-discussed slab – at a low temperature $T = 0.001J$ and in-plane magnetic field $H_{in} = 0.3J$, with the DM vectors lying in the x - y plane. These domains were obtained here as metastable solutions of the MC evolutions. Typical spatial profiles of the scalar spin chirality χ , as in Fig. 4(b), present pronounced features at the boundaries between the labyrinth domains. Therefore, this finite scalar spin chirality at the boundaries can produce a topological Hall effect even at zero magnetic field [23].

In an in-plane magnetic field, after subtracting the zero-field contribution arising from the domain boundaries, we find that the transverse Hall conductivity, MC-averaged over several domain configurations, exhibits a four-fold symmetry with respect to the field angle θ , as depicted in Fig. 4(c). The four minima in $|\sigma_{xy} - \sigma_{xy}(H_{in} = 0)|$ appears at $\theta = (2n - 1) \times 45^\circ$, ($n = 1, 2, 3, 4$). For the CSS texture having only one diagonal arrangement, as presented in Fig. 2(a), if the applied magnetic field induces a reorientation of the stripes [34, 35], σ_{xy} is also expected to reveal a four-fold symmetric θ -dependence. The formation of the labyrinth domains is not possible with the IST since they only appear perpendicular to the plane of the DM vectors, typically fixed in a given material. Therefore, the observation of such a four-fold symmetric PTHE can convincingly identify the CSS texture and exclude the other possibility of IST texture.

Discussion.—We discussed DM interactions that are 2D in nature and the resulting spiral and skyrmions are Néel-type textures. This consideration is prevalent in either effective 2D systems such as oxide interfaces or bulk 3D systems with DM vectors lying identically in parallel 2D planes. Moreover, for a DM interaction that has both in-plane and out-of-plane components, the resulting textures are Bloch type [6–8]. The description of PTHE, presented here, is equally applicable for the Bloch-type magnetic textures as well.

To conclude, we propose *the emergence of topological Hall effect from conical spin spiral textures*, when the magnetic field, charge current, and DM vectors all lie in the same plane. The PTHE generically develops from the real-space Berry curvature of the conical spiral spin texture and it appears in a wide variety of magnetic materials. We outline the distinguishing features of the planar topological Hall response from two possible sources, namely the in-plane skyrmions and the conical spin spirals, which can be important to unambiguously probe chiral magnetic textures and identify the nature of the antisymmetric spin-exchange interaction.

Acknowledgements.—This work was supported by the U.S. Department of Energy (DOE), Office of Science, Basic Energy Sciences (BES), Materials Sciences and Engineering Division.

- * Copyright notice. This manuscript has been authored by UTBattelle, LLC under Contract No. DE-AC05-00OR22725 with the U.S. Department of Energy. The United States Government retains and the publisher, by accepting the article for publication, acknowledges that the United States Government retains a non-exclusive, paid-up, irrevocable, world-wide license to publish or reproduce the published form of this manuscript, or allow others to do so, for United States Government purposes. The Department of Energy will provide public access to these results of federally sponsored research in accordance with the DOE Public Access Plan (<http://energy.gov/downloads/doepublic-access-plan>)
† Email: mohantan@ornl.gov
- [1] N. Nagaosa and Y. Tokura, “Topological properties and dynamics of magnetic skyrmions,” *Nat. Nanotechnol.* **8**, 899 (2013).
 - [2] L. D. Barron, “Chirality and magnetism shake hands,” *Nat. Mater.* **7**, 691 (2008).
 - [3] A. Fert, N. Reyren, and V. Cros, “Magnetic skyrmions: advances in physics and potential applications,” *Nat. Rev. Mater.* **2**, 17031 (2017).
 - [4] U. K. Röföler, A. N. Bogdanov, and C. Pfleiderer, “Spontaneous skyrmion ground states in magnetic metals,” *Nature* **442**, 797 (2006).
 - [5] X. Li, W. V. Liu, and L. Balents, “Spirals and skyrmions in two dimensional oxide heterostructures,” *Phys. Rev. Lett.* **112**, 067202 (2014).
 - [6] A. Neubauer, C. Pfleiderer, B. Binz, A. Rosch, R. Ritz, P. G. Niklowitz, and P. Böni, “Topological Hall effect in the A phase of MnSi,” *Phys. Rev. Lett.* **102**, 186602 (2009).
 - [7] S. Mühlbauer, B. Binz, F. Jonietz, C. Pfleiderer, A. Rosch, A. Neubauer, R. Georgii, and P. Böni, “Skyrmion lattice in a chiral magnet,” *Science* **323**, 915 (2009).
 - [8] X. Z. Yu, Y. Onose, N. Kanazawa, J. H. Park, J. H. Han, Y. Matsui, N. Nagaosa, and Y. Tokura, “Real-space observation of a two-dimensional skyrmion crystal,” *Nature* **465**, 901 (2010).
 - [9] S. Heinze, K. von Bergmann, M. Menzel, J. Brede, A. Kubetzka, R. Wiesendanger, G. Bihlmayer, and S. Blügel, “Spontaneous atomic-scale magnetic skyrmion lattice in two dimensions,” *Nat. Phys.* **7**, 713 (2011).
 - [10] X. Z. Yu, N. Kanazawa, Y. Onose, K. Kimoto, W. Z. Zhang, S. Ishiwata, Y. Matsui, and Y. Tokura, “Near room-temperature formation of a skyrmion crystal in thin-films of the helimagnet FeGe,” *Nat. Mater.* **10**, 106 (2011).
 - [11] N. Kanazawa, Y. Onose, T. Arima, D. Okuyama, K. Ohoyama, S. Wakimoto, K. Kakurai, S. Ishiwata, and Y. Tokura, “Large topological Hall effect in a short-period helimagnet MnGe,” *Phys. Rev. Lett.* **106**, 156603 (2011).
 - [12] S. X. Huang and C. L. Chien, “Extended skyrmion phase in epitaxial FeGe(111) thin films,” *Phys. Rev. Lett.* **108**, 267201 (2012).
 - [13] T. Schulz, R. Ritz, A. Bauer, M. Halder, M. Wagner, C. Franz, C. Pfleiderer, K. Everschor, M. Garst, and A. Rosch, “Emergent electrodynamics of skyrmions in a chiral magnet,” *Nat. Phys.* **8**, 301 (2012).
 - [14] H. S. Park, X. Yu, S. Aizawa, T. Tanigaki, T. Akashi, Y. Takahashi, T. Matsuda, N. Kanazawa, Y. Onose, D. Shindo, A. Tonomura, and Y. Tokura, “Observation of the magnetic flux and three-dimensional structure of skyrmion lattices by electron holography,” *Nat. Nanotechnol.* **9**, 337 (2014).
 - [15] J. Matsuno, N. Ogawa, K. Yasuda, F. Kagawa, W. Koshibae, N. Nagaosa, Y. Tokura, and M. Kawasaki, “Interface-driven topological Hall effect in SrRuO₃-SrIrO₃ bilayer,” *Sci. Adv.* **2**, e1600304 (2016).
 - [16] M. Nakamura, D. Morikawa, X. Yu, F. Kagawa, T. Arima, Y. Tokura, and M. Kawasaki, “Emergence of topological Hall effect in half-metallic manganite thin films by tuning perpendicular magnetic anisotropy,” *J. Phys. Soc. Jpn.* **87**, 074704 (2018).
 - [17] L. Vistoli, W. Wang, A. Sander, Q. Zhu, B. Casals, R. Cicheler, A. Barthélémy, S. Fusil, G. Herranz, S. Valencia, R. Abrudan, E. Weschke, K. Nakazawa, H. Kohno, J. Santamaria, W. Wu, V. Garcia, and M. Bibes, “Giant topological Hall effect in correlated oxide thin films,” *Nat. Phys.* **15**, 67 (2019).
 - [18] T. Yokouchi, N. Kanazawa, A. Tsukazaki, Y. Kozuka, A. Kikkawa, Y. Taguchi, M. Kawasaki, M. Ichikawa, F. Kagawa, and Y. Tokura, “Formation of in-plane skyrmions in epitaxial MnSi thin films as revealed by planar Hall effect,” *J. Phys. Soc. Jpn.* **84**, 104708 (2015).
 - [19] S. Banerjee, O. Erten, and M. Randeria, “Ferromagnetic exchange, spin-orbit coupling and spiral magnetism at the LaAlO₃/SrTiO₃ interface,” *Nat. Phys.* **9**, 626 (2013).
 - [20] W. Jiang, S. Zhang, X. Wang, C. Phatak, Q. Wang, W. Zhang, M. B. Jungfleisch, J. E. Pearson, Y. Liu, J. Zang, X. Cheng, A. Petford-Long, A. Hoffmann, and S. G. E. te Velthuis, “Quantifying chiral exchange interaction for Néel-type skyrmions via Lorentz transmission electron microscopy,” *Phys. Rev. B* **99**, 104402 (2019).
 - [21] N. Mohanta, E. Dagotto, and S. Okamoto, “Topological Hall effect and emergent skyrmion crystal at manganite-iridate oxide interfaces,” *Phys. Rev. B* **100**, 064429 (2019).
 - [22] N. Nagaosa, X. Z. Yu, and Y. Tokura, “Gauge fields in real and momentum spaces in magnets: monopoles and skyrmions,” *Phil. Trans. R. Soc. A* **370**, 5806 (2012).
 - [23] For additional information, see the Supporting Information.
 - [24] M. Ezawa, “Compact merons and skyrmions in thin chiral magnetic films,” *Phys. Rev. B* **83**, 100408 (2011).
 - [25] S. Buhrandt and L. Fritz, “Skyrmion lattice phase in three-dimensional chiral magnets from Monte Carlo simulations,” *Phys. Rev. B* **88**, 195137 (2013).
 - [26] M. N. Wilson, A. B. Butenko, A. N. Bogdanov, and T. L. Monchesky, “Chiral skyrmions in cubic helimagnet films: The role of uniaxial anisotropy,” *Phys. Rev. B* **89**, 094411 (2014).
 - [27] T.-E. Park, L. Peng, J. Liang, A. Hallal, X. Zhang, S. Jong Kim, K. M. Song, K. Kim, M. Weigand, G. Schuetz, S. Finizio, J. Raabe, J. Xia, Y. Zhou, M. Ezawa, X. Liu, J. Chang, H. C. Koo, Y. Duck Kim, M. Chshiev, A. Fert, H. Yang, X. Yu, and S. Woo, “Observation of magnetic skyrmion crystals in a van der Waals ferromagnet Fe₃GeTe₂,” [arXiv:1907.01425](https://arxiv.org/abs/1907.01425) (2019).
 - [28] Y. You, Y. Gong, H. Li, Z. Li, M. Zhu, J. Tang, E. Liu, Y. Yao, G. Xu, F. Xu, and W. Wang, “Planar topological Hall effect in a uniaxial van der Waals ferromagnet Fe₃GeTe₂,” [arXiv:1907.02397](https://arxiv.org/abs/1907.02397) (2019).

- [29] M. Seul and R. Wolfe, “Evolution of disorder in magnetic stripe domains. II. hairpins and labyrinth patterns versus branches and comb patterns formed by growing minority component,” *Phys. Rev. A* **46**, 7534 (1992).
- [30] A. Kashuba and V. L. Pokrovsky, “Stripe domain structures in a thin ferromagnetic film,” *Phys. Rev. Lett.* **70**, 3155 (1993).
- [31] O. Portmann, A. Vaterlaus, and D. Pescia, “An inverse transition of magnetic domain patterns in ultrathin films,” *Nature* **422**, 701 (2003).
- [32] N. Saratz, A. Lichtenberger, O. Portmann, U. Ramsperger, A. Vindigni, and D. Pescia, “Experimental phase diagram of perpendicularly magnetized ultrathin ferromagnetic films,” *Phys. Rev. Lett.* **104**, 077203 (2010).
- [33] S. Woo, K. Litzius, B. Krüger, M.-Y. Im, L. Caretta, K. Richter, M. Mann, A. Krone, R. M. Reeve, M. Weigand, P. Agrawal, I. Lemesh, M.-A. Mawass, P. Fischer, M. Kläui, and G. S. D. Beach, “Observation of room-temperature magnetic skyrmions and their current-driven dynamics in ultrathin metallic ferromagnets,” *Nat. Mater.* **15**, 501 (2016).
- [34] S. Fin, R. Tomasello, D. Bisero, M. Marangolo, M. Sacchi, H. Popescu, M. Eddrief, C. Hepburn, G. Finocchio, M. Carpentieri, A. Rettori, M. G. Pini, and S. Tacchi, “In-plane rotation of magnetic stripe domains in $\text{Fe}_{1-x}\text{Ga}_x$ thin films,” *Phys. Rev. B* **92**, 224411 (2015).
- [35] A. D. Kent, J. Yu, U. Rüdiger, and S. S. P. Parkin, “Domain wall resistivity in epitaxial thin film microstructures,” *J. Phys. Condens. Matter.* **13**, R461 (2001).

Supplemental Material

1. Monte Carlo calculation. To obtain the spin texture of the slab of size $20 \times 20 \times 10$, we consider periodic boundary conditions along all three directions. We started the MC calculation at a high temperature $T = 5J$ with a completely random spin configuration and lowered the temperature very slowly down to a very low value $T = 0.001J$. We used 1000 temperature steps and at each temperature, we performed 2×10^6 MC spin updates. In each MC update, the spin angle – either the polar angle θ' or the azimuthal angle ϕ' – is changed to $\theta' \pm 5^\circ$ or $\phi' \pm 5^\circ$, respectively (the sign is also chosen randomly) and the new spin configuration was accepted or rejected according to the Metropolis algorithm [21].

In the presence of the in-plane magnetic field, we performed 2×10^6 additional steps of MC evolutions at each field angle θ , keeping the temperature fixed at $T = 0.001J$, starting with the spin configuration which had been obtained by MC annealing at zero field. The labyrinth stripe domains presented here are metastable solutions of the MC evolution.

2. Topological Hall effect from Labyrinth domains.

In Fig. S1(a) and (c), we show the spin configurations with zero magnetic field and with an out-of-plane magnetic field $H_z = 0.8J$, in a two-dimensional 20×20 cluster. The real-space profile of the scalar spin chirality χ for these two spin configurations are shown in Figs. S1(b) and (d). Unlike the

skyrmion crystal phase, the “normal” spin spiral has a negligible scalar chirality and, therefore, does not produce any topological Hall effect. Figures S1(e) and (f) are the plots of the spin texture and scalar spin chirality profiles, respectively, on a 40×40 cluster, showing the labyrinth domains and their influence on the scalar spin chirality in the absence of any magnetic field. Such stripe domains are expected to produce topological Hall effect even in the absence of any external magnetic field.

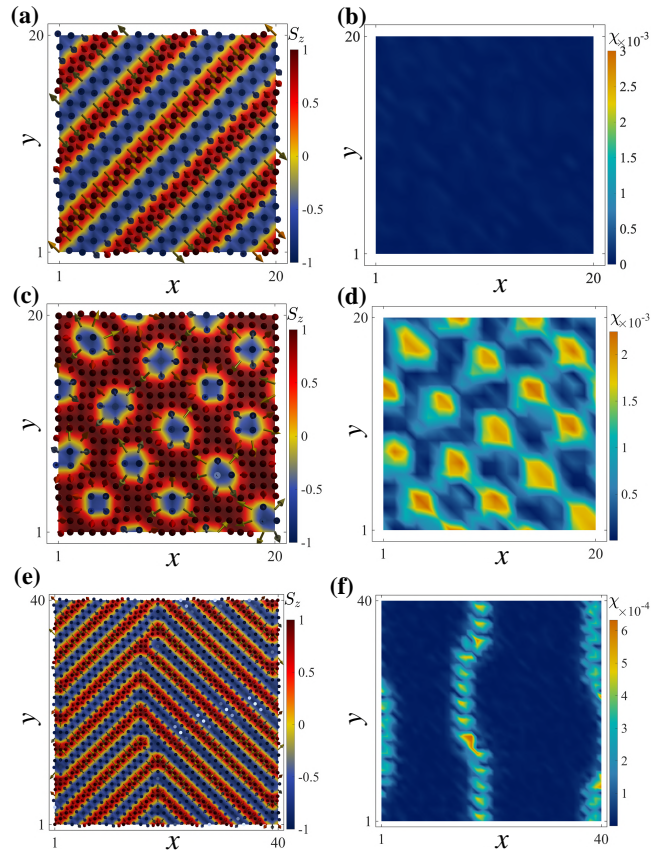


FIG. S1. (a) Spiral spin texture of a 20×20 cluster with in-plane DM vector in the absence of magnetic field. (b) Spatial profile of the scalar spin chirality χ for the spiral spin texture shown in panel (a). (c) Skyrmion crystal stabilized at an out-of-plane magnetic field $H_z = 0.8J$. (d) Spatial profile of χ corresponding to the skyrmion crystal shown in (c). (e) Spiral spin texture with two mutually-orthogonal stripes coexisting in a 40×40 cluster with in-plane DM vector in the absence of magnetic field. (f) Profile of the scalar spin chirality χ for the spiral spin texture shown in plot (e). In all panels, parameters used are Heisenberg exchange $J = 1$, DM interaction strength $D = \sqrt{6}$, temperature $T = 0.001$, and easy-plane anisotropy $A = 0.01$ [21].